analytical chemistry

pubs.acs.org/ac Article

A Pyroglutamate Aminopeptidase 1 Responsive Fluorescence Imaging Probe for Real-Time Rapid Differentiation between Thyroiditis and Thyroid Cancer

Siqi Zhang, Mo Ma, Jingkang Li, Jiaxin Li, Lanlan Xu, Dejiang Gao, Pinyi Ma,* Hui Han,* and Daqian Song*

Cite This: *Anal. Chem.* 2024, 96, 5897−5905 Read Online

ACCESS | Metrics & More | Article Recommendations | Supporting Information

ABSTRACT: Current diagnostic methods for thyroid diseases, including blood tests, ultrasound, and biopsy, always have difficulty diagnosing thyroiditis accurately, occasionally mistaking it for thyroid cancer. To address this clinical challenge, we developed Ox-PGP1, a novel fluorescent probe realizing rapid, noninvasive, and real-time diagnostic techniques. This is the first imaging tool capable of noninvasively distinguishing between thyroiditis and thyroid cancer. Ox-PGP1 was introduced as a fluorescent probe custom-built for the specific detection and quantification of pyroglutamate aminopeptidase 1 (PGP-1), a known pivotal biomarker of inflammation. Ox-PGP1 overcame the disadvantages of traditional enzyme-responsive fluorescent probes that relied on the intramolecular charge transfer (ICT) mechanism, including the issue of high background fluorescence, while offering exceptional photostability under laser irradiation. The spectral properties of Ox-PGP1 were meticulously optimized to enhance its biocompatibility. Furthermore, the low limit of detection (LOD) of Ox-PGP1 was determined to be 0.09 μg/mL, which demonstrated its remarkable sensitivity and precision. Both cellular and *in vivo* experiments validated the capacity of Ox-PGP1 for accurate differentiation between normal, inflammatory, and cancerous thyroid cells. Furthermore, Ox-PGP1 showed the potential to rapidly and sensitively differentiate between autoimmune thyroiditis and anaplastic thyroid carcinoma in a mouse model, achieving results in just 5 min. The successful design and application of Ox-PGP1 represent a substantial advancement in technology over traditional diagnostic approaches, potentially enabling earlier interventions for thyroid diseases.

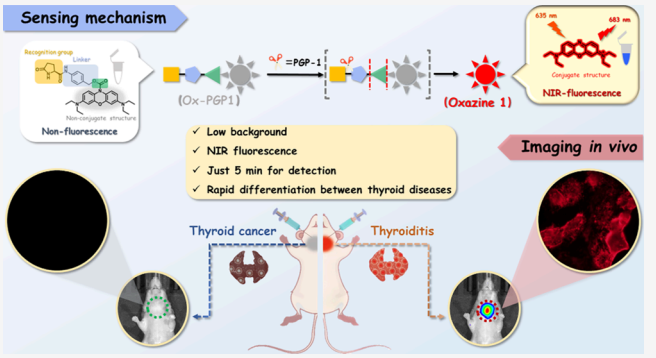

INTRODUCTION

Autoimmune thyroiditis, a chronic autoimmune condition, is characterized by the constant disruption of thyroid gland function stemming from an attack by immune cells of the host on its own tissues.[1,2] As the disease progresses, it not only threatens health via potential complications such as membranous nephropathy, glomerulonephritis, and nephrotic syndrome but also heightens the risk of thyroid cancer.[3−9] In the unfortunate event that it develops into extremely rare anaplastic thyroid carcinoma, it could become even more life-threatening.[10] However, the insidious onset and slow progression always make most patients remain asymptomatic, making the diseases undetected, in turn underscoring the necessity for efficacious diagnostic measures.[11,12]

Current medical technologies for diagnosing thyroid diseases typically include blood sampling, ultrasound, and biopsy.[13−15] However, traditional noninvasive methods are incapable of complete and accurate diagnosing thyroiditis under certain conditions and may inadvertently misdiagnose thyroiditis as thyroid cancer.[16,17] In instances of inconclusive ultrasound results, patients undergo painful biopsy procedures and endure lengthy waits for pathology reports, which not only delay the diagnosis but also sometimes lead to misdiagnosis.[18] These pessimistic circumstances underscore the necessity for swift, noninvasive, and real-time differentiation between thyroiditis and thyroid cancer. Fluorescence imaging, characterized by rapid, nondestructive detection, high sensitivity, superior resolution, and minimal toxicity, could be a promising solution that can address these issues.[19−24] Therefore, it may play a critical role in diagnosing and identifying diseases tied to the target organs. However, until now, there is no fluorescence

Received: December 22, 2023
Revised: February 26, 2024
Accepted: March 21, 2024
Published: April 1, 2024

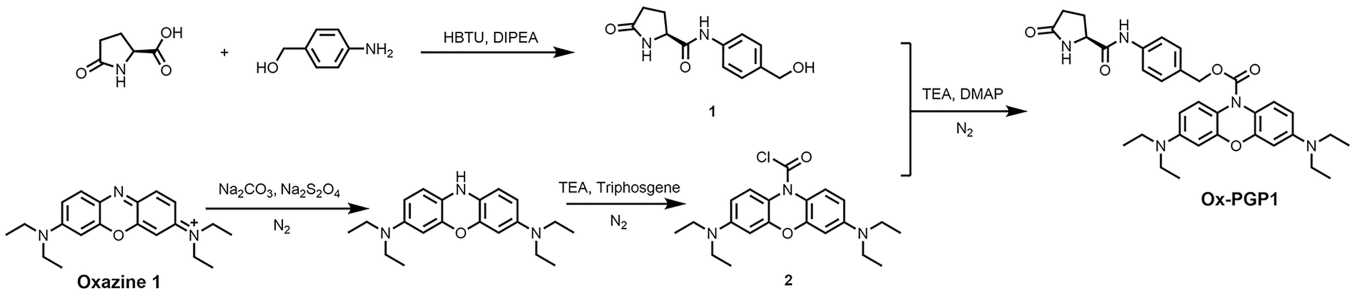

Figure 1. Synthesis Process of Ox-PGP1.

imaging method for the effective analysis of autoimmune thyroiditis.

Recent developments have highlighted PGP-1 as a potential marker suitable for detecting inflammation due to the important role of PGP-1 in the pathways of inflammatory processes.[25−27] PGP-1, which is tripeptidyl aminopeptidase that cleaves the N-terminal pyroglutamate peptide bond of proteins, has been shown to associate with cellular immune responses, and thus could potentially serve as a novel cellular inflammation indicator.[28−32] Consequently, the development of innovative PGP-1 probes for fluorescence imaging could provide a novel approach for diagnosing targeted organ inflammation and differentiating inflammation from cancer.

In this work, we designed the fluorescent probe Ox-PGP1 for targeting and monitoring the concentration of PGP-1 in thyroiditis. By interrupting the conjugated structure of the oxazine 1 dye, this innovative probe was able to address the known defect of most enzyme-responsive fluorescent probes based on the ICT mechanism, such as high background signals. To develop a near-infrared fluorescent probe for the specific detection of PGP-1, 4-aminobenzyl alcohol was introduced as the self-eliminating group, and L-pyroglutamic acid was attached to the self-eliminating group through covalent bonds. The probe Ox-PGP1 exhibited robust photostability and could resist decomposition under laser irradiation. We optimized the spectral properties of Ox-PGP1 for its biocompatibility and verified its capability to specifically recognize PGP-1 without interference from other biological substances. Cell experiments demonstrated that Ox-PGP1 could effectively distinguish between normal thyroid cells, inflammatory thyroid cells, and various types of cancerous thyroid cells. Moreover, it was proven to be effective in screening for the best medicine for thyroiditis. The successful fluorescence imaging of autoimmune thyroiditis and anaplastic thyroid carcinoma mice model confirmed that Ox-PGP1 had a potential in rapid and sensitive differentiation between two different thyroid disorders in only 5 min.

EXPERIMENTAL PROCEDURE

Materials and Instruments. Details of the materials and instruments used in this work can be found in the Supporting Information (SI) section.

Probe synthesis. The synthesis process of Ox-PGP1 is described in Figure 1.

Compound **1**. L-Pyroglutamic acid (645 mg, 5 mmol), *O*-benzotriazole-*N*,*N*,*N*′,*N*′-tetramethyl-uronium-hexafluorophosphate (HBTU, 1.9 g, 5 mmol), and *N*-ethyldiisopropylamine (DIPEA, 0.9 mL, 5 mmol) were dissolved in 20 mL of anhydrous tetrahydrofuran (THF). Subsequently, 4-aminobenzyl alcohol (615 mg, 10 mmol), dissolved in anhydrous THF, was added dropwise to the reaction mixture. The reaction was maintained below 0 °C and continuously stirred for 10 min. Thereafter, the reaction mixture was allowed to warm to room temperature and was stirred for another 5 h. The solvent was subsequently removed via vacuum distillation, and the resulting crude product was purified by silica gel chromatography using dichloromethane and methanol (v/v, 50:1) as the eluent. This process yielded compound **1** as a white solid (0.84 g, 72% yield). ^{1}H NMR (300 MHz, DMSO-d_6) δ 10.02 (s, 1H), 7.89 (s, 1H), 7.56 (d, J = 8.5 Hz, 2H), 7.25 (d, J = 8.5 Hz, 2H), 5.12 (t, J = 5.7 Hz, 1H), 4.43 (d, J = 5.6 Hz, 2H), 4.17 (dd, J = 8.3, 4.2 Hz, 1H), 2.53−1.86 (m, 8H) (Figure S1). HR-MS (m/z): Calculated for $[C_{12}H_{15}N_2O_3]^+$: 235.1077; found: 237.1078 (Figure S2).

Compound **2**. The methodology used in the synthesis of compound **2** was adopted from the previous literature.[33,34] Oxazine 1 (700 mg, 0.5 mmol) and sodium carbonate (Na_2CO_3, 212 mg, 2.0 mmol) were dissolved in 7.0 mL of water under a nitrogen atmosphere, followed by the addition of dichloromethane (CH_2Cl_2, 6 mL). Sodium dithionite ($Na_2S_2O_4$, 409 mg, 2.0 mmol), dissolved in 10 mL of water, was then slowly added to the solution. The reaction mixture was continuously stirred at 40 °C for 1 h. Subsequently, triethylamine (100 μL, 0.7 mmol) was added dropwise under the same nitrogen atmosphere, and the reaction temperature was reduced to below 0 °C. Bis(trichloromethyl) carbonate (100 mg, 0.3 mmol), dissolved in 5 mL of CH_2Cl_2, was then added slowly to the reaction mixture. The reaction mixture was further stirred at 40 °C for 1 h before being subjected to extraction with CH_2Cl_2. The organic layer was isolated as fast as possible and dried over anhydrous sodium sulfate (Na_2SO_4). The solvent was then removed under reduced pressure within 30 °C to yield compound 2 as a light green solid (0.14 g, 72% yield). The resultant crude intermediate was immediately and directly used in the subsequent reaction without further purification.

Ox-PGP1. Under a nitrogen atmosphere, compound **2** (140 mg, 0.36 mmol) was combined with compound **1** (94 mg, 0.4 mmol) in a solution containing pyridine (2 mL) and 4-dimethylaminopyridine (DMAP, 120 mg, 1.0 mmol). The mixture was stirred at 45 °C for 1 h. Afterward, the solvent was removed via reduced-pressure distillation, and the remaining residue was further purified by silica gel chromatography using petroleum ether and ethyl acetate (v/v, 50:1) as the eluent. This process yielded the probe Ox-PGP1 as a blue solid product (63 mg, 30% yield). ^{1}H NMR (300 MHz, $CDCl_3$) δ 8.43 (s, 1H), 7.59 (d, J = 8.2 Hz, 2H), 7.43−7.29 (m, 4H), 6.85 (s, 1H), 6.35 (d, J = 2.3 Hz, 4H), 5.22 (s, 2H), 4.29−4.15 (m, 1H), 3.32 (q, J = 7.0 Hz, 8H), 2.68−2.20 (m, 4H), 1.15 (t, J = 7.0 Hz, 12H) (Figure S3). ^{13}C NMR (75 MHz, $CDCl_3$) δ

https://doi.org/10.1021/acs.analchem.3c05872
Anal. Chem. 2024, 96, 5897−5905

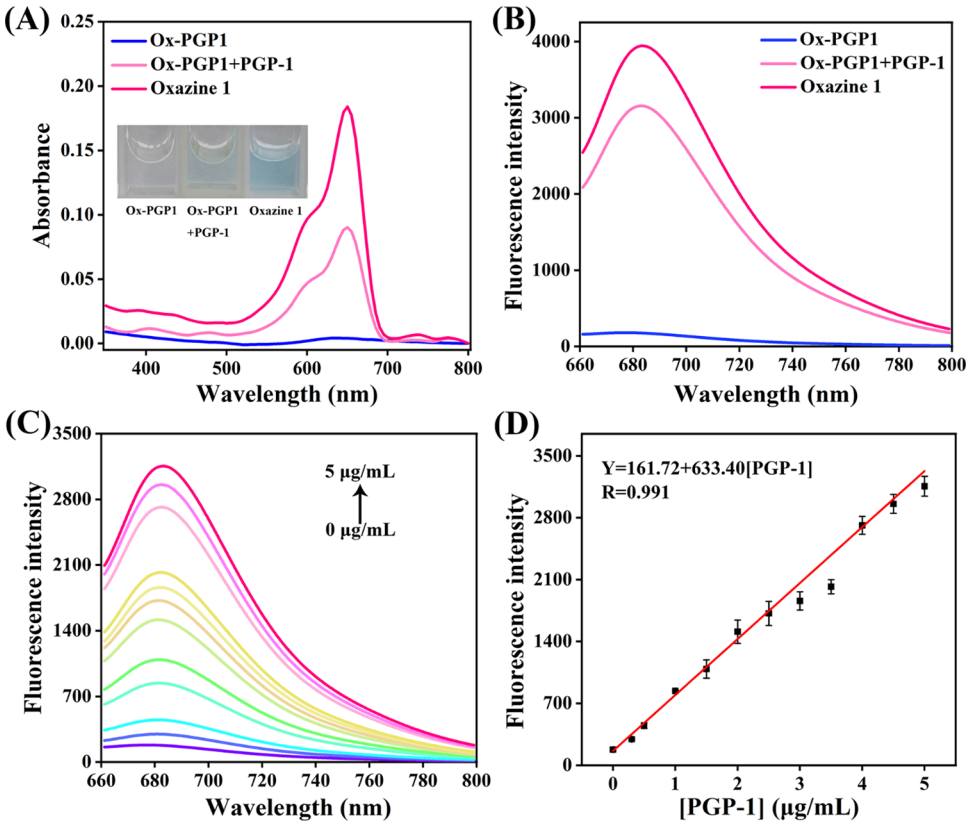

Figure 2. (A) UV−vis absorption spectra of Ox-PGP1 (10 μM), the reaction system, and oxazine 1 (10 μM). (B) Fluorescence spectra of Ox-PGP1 (10 μM), the reaction system, and oxazine 1 (10 μM), λ_{ex} = 635 nm. (C) Fluorescence spectra of Ox-PGP1 following the gradual addition of PGP-1, λ_{ex} = 635 nm. (D) Linear relationship between fluorescence intensity (I_{683}) of Ox-PGP1 and PGP-1 concentration (0−5 μg/mL), λ_{ex} = 635 nm.

179.38, 170.59, 153.67, 151.22, 146.28, 137.54, 132.41, 128.81, 125.09, 120.13, 106.38, 99.34, 67.42, 57.72, 44.58, 29.67, 25.62, 12.46 (Figure S4). HR-MS (m/z): Calculated for $[C_{33}H_{40}N_5O_5]^+$: 586.3024, found: 586.3023 (Figure S5).

Preparation of Samples for Spectrophotometric Analysis. The Ox-PGP1 stock solution (1 mM in DMSO) was prepared and stored in a light-protected environment at −40 °C. PGP-1 was dissolved in sterilized water to a final concentration of 50 μg/mL, and then it was stored in a −80 °C freezer for future use. Thereafter, the Ox-PGP1 stock solution was further dissolved in phosphate-buffered saline (PBS, pH = 7.4, 10 mM), and PGP-1 solution at various volumes were added to achieve the desired concentration. The volumes of PBS, Ox-PGP1, and PGP-1 solutions were maintained at 300 μL. A control group was prepared without PGP-1. All samples were then incubated on a 37 °C shaker for 2 h before subsequent *in vitro* assays. Finally, the fluorescence emission spectra and UV−vis absorption spectra were obtained at 37 °C using a 1 cm quartz cuvette. The excitation and emission slits widths were set at 10 nm (λ_{ex} = 635 nm, PMT = 700 V).

Autoimmune Thyroiditis Mice Imaging Experiment. The animal experiment was carried out under the ethical protocols set by Jilin University's Institutional Animal Care and Use Committee (IACUC), certified by ethical inspection permit number SY202306031.

Establishing the autoimmune thyroiditis mice model:[35] A water-in-oil emulsion was prepared by mixing porcine thyroglobulin (PTg) with complete Freund's adjuvant (v/v, 1:1) to a final concentration of 0.25 mg/mL. The resulting emulsion was administered at multiple injection points underneath the dorsal skin of the mice at a total dose of 50 μg/animal. The injections were performed once per week over a two-week period. From the third week onward, the water-in-oil emulsion was replaced by mixing porcine thyroglobulin (PTg) with incomplete Freund's adjuvant (v/v, 1:1) to a final concentration of 0.25 mg/mL and dosage for 3 weeks. The resulting emulsion was administered at multiple injection points at a total dose of 50 μg/animal, as well. The injection sites included the subcutaneous dorsal, neck, and abdominal cavity regions. Concurrently, mice were provided with high iodine content (0.63 mg/mL).

The 8305C cell suspension (containing approximately 1 × 10^7 cells dissolved in 50 μL of PBS) was subcutaneously injected into the thyroid gland of mice, and the tumors were allowed to grow for approximately 2 weeks.

For imaging, Ox-PGP1 (60 μM, 200 μL) was injected near the neck region of the model mice with autoimmune thyroiditis and anaplastic thyroid carcinoma. Fluorescence imaging was conducted every ten min postinjection (with the mice being anesthetized with isoflurane). The control group was treated with Ox-PGP1 injections in an identical manner, and imaging was performed using a small animal imager.

RESULTS AND DISCUSSION

Molecular Design of Ox-PGP1. Oxazine 1, a commercially available NIR dye derived from phenoxazine, exhibits a rigid conjugated structure. In the actual chemical reaction, $Na_2S_2O_4$ was added to the oxazine 1 dye as a reducing agent to

https://doi.org/10.1021/acs.analchem.3c05872
Anal. Chem. 2024, 96, 5897−5905

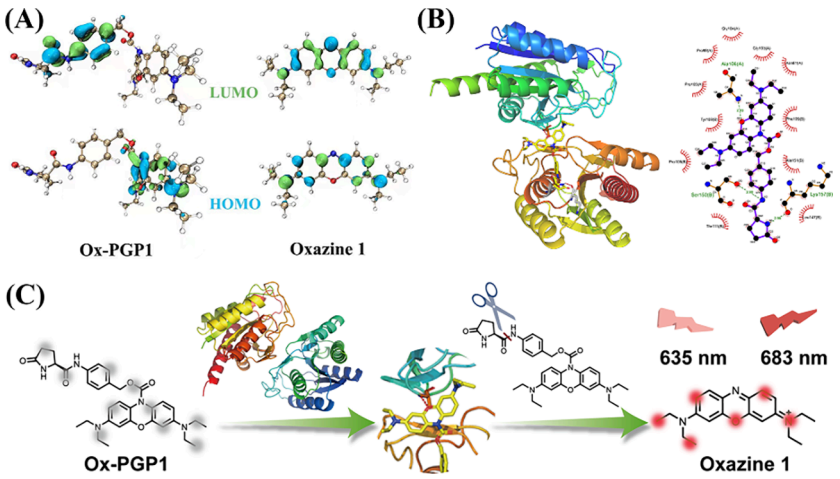

Figure 3. (A) Ground state geometries and electronic structures of Ox-PGP1 and oxazine 1. (B) Simulation of interactions between Ox-PGP1 and PGP-1. (C) Sensing mechanism of Ox-PGP1 for PGP-1.

disrupt the conjugated network of the oxazine 1 dye. This led to an almost negligible UV−vis absorption light and extremely low fluorescence, which were the highlights of the design of the fluorophore. Almost all other methods for PGP-1 detection mentioned in Table S1 were based on the ICT mechanism. Compared to the above-reported literature, Ox-PGP1 broke the inherent design mechanism and realized the nonconjugated fundamental chemical structure. It represented a more advanced method in enzyme-responsive fluorescent probe design, especially in offering lower background fluorescence by interrupting the conjugated structure of the oxazine 1 dye, which greatly solved the problem of poor quenching of the probe. To facilitate the fluorophore functionalization, a linker group, 4-aminobenzyl alcohol, was integrated into the structure. It not only provided an amino group to the link of the recognition group but also ensured that the recognition group of the molecular substrate could access and bind to the active center of PGP-1. Without PGP-1 digestion, the conjugated structure of Ox-PGP1 molecule was fully disrupted, resulting in minimal fluorescence intensity. Upon the introduction of PGP-1, it interacted with the recognition group of Ox-PGP1 and cleaved the amide bond. Concurrently, the linking group was self-eliminated and culminated during the production of oxazine 1, a compound characterized by its intense fluorescence emission and a property of near-infrared emission. Thus, an effective NIR dye-based probe Ox-PGP1 with low background fluorescence could be realized through the functionalization of oxazine 1, the controlled PGP-1 interaction and subsequent fluorescence emission, further allowing for more accurate and sensitive detection in biological applications.

Spectral Characterization before and after PGP-1 Digestion. To begin, we scrutinized the UV−vis absorption spectra of Ox-PGP1 before and after PGP-1 digestion. As depicted in Figure 2A, the Ox-PGP1 system without PGP-1 was transparent and colorless and exhibited a very faint absorption peak at 635 nm. In the presence of PGP-1 at a concentration of 5 μg/mL, however, the system color transitioned from colorless to blue and a conspicuous enhancement of the absorption peak at 635 nm was observed. This phenomenon aligned with the conversion of Ox-PGP1 to oxazine 1 upon PGP-1 degradation. As demonstrated in Figure 2B, the fluorescence spectra followed a similar trend to the UV−vis absorption spectra: a significant increase in the fluorescence intensity of the peak at 683 nm compared to that without PGP-1. Upon continuous irradiation with 635 nm excitation light, the fluorescence intensity of Ox-PGP1 remained largely unchanged, suggesting that Ox-PGP1 in the reaction system could resist decomposition and maintain its stable molecular structure (Figure S6). Furthermore, the mass spectral analysis postreaction between Ox-PGP1 and PGP1, as shown in Figure S7, revealed a peak at m/z = 324.2074 corresponding to oxazine 1 (m/z = 324.2070). Thus, the UV−vis absorption spectra, the fluorescence spectra, and the HR-MS spectrum validated the transformation of Ox-PGP1 to oxazine 1, as well as corroborated its stability and resistance to decomposition, which reinforced its potential for use in reaction systems under conditions with continuous excitation.

Conditional Screening. In the study of reaction time, when the PGP-1 concentration reached 5 μg/mL, a distinct fluorescence peak was observed at 2 h. After this time, the fluorescence intensity remained stable (Figure S8). This suggests that 2 h is the optimal time for the interaction between Ox-PGP1 and PGP-1, and any further extension of the reaction time has no effect on fluorescence intensity.

As shown in Figure S9, it was apparent that neutral or alkaline conditions could enhance the fluorescence intensity of the system. Given the typical pH condition in the microenvironment of organisms, a pH of 7.4 was chosen as the optimal reaction pH. It was noteworthy that both Ox-PGP1 and oxazine 1 were able to attain nearly all of their maximum fluorescence intensities at this pH.

Furthermore, the exploration of temperature effects revealed that the temperature of 37 °C led to a significant increase in fluorescence compared to 25, 30, and 43 °C. This implies that the optimal response conditions for Ox-PGP1 align with the optimal temperature of organism microenvironment, an indication that Ox-PGP1 is suitable for subsequent biological experiments (Figure S10).

Linear Response and the Kinetic of the Enzymatic Reaction. We observed that the fluorescence intensity of the system at an excitation wavelength of 635 nm exhibited a nearly 18-fold increase in the signal when the PGP-1 concentration was escalated from 0 to 5 μg/mL (Figure 2C). The increase in fluorescence intensity not only was dramatic but also was linearly correlated with PGP-1 concentration from

https://doi.org/10.1021/acs.analchem.3c05872
Anal. Chem. 2024, 96, 5897−5905

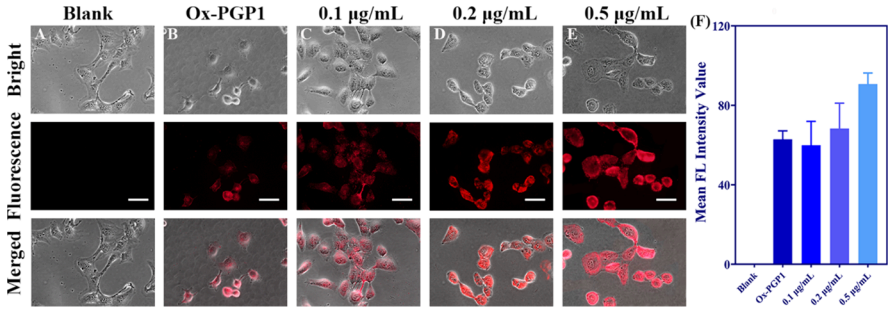

Figure 4. Fluorescence imaging of Nthy-ori3−1 cells under various conditions: (A) untreated cells; (B) cells after 40 min of incubation with 10 μM Ox-PGP1; (C) cells post 16 h incubation with 0.1 μg/mL LPS, followed by a 40 min treatment with 10 μM Ox-PGP1; (D) cells post 16 h incubation with 0.2 μg/mL LPS, followed by a 40 min treatment with 10 μM Ox-PGP1; (E) cells post 16 h incubation with 0.5 μg/mL LPS, followed by a 40 min treatment with 10 μM Ox-PGP1. (F) Comparison of the fluorescence intensities obtained under the above conditions. λex = 605−640 nm, λem = 670−715 nm. Scale bar, 50 μm.

0 to 5 μg/mL (Figure 2D). Furthermore, the LOD of Ox-PGP1, calculated using the $3\sigma/k$ formula, was 0.09 μg/mL. Further, the kinetic of the enzymatic reaction was investigated using the Michaelis−Menten plot and Lineweaver−Burk plot. As shown in Figure S11, V_{max} = 20.59 μM min^{-1} and K_m = 0.54 μM. The results indicated that Ox-PGP1 had good affinity and high sensitivity to PGP-1 (Figure S11). In conclusion, the findings presented above underscore the potential of Ox-PGP1 in effectively interacting with PGP-1, further illuminating its potential utilization in precise and quantitative measurements.

Selectivity and Inhibitor Screening. The selectivity response of Ox-PGP1 was further explored. The selectivity of Ox-PGP1 was conducted to determine the influence of 49 common biological substances, including anions, cations, amino acids, and various enzymes, on the probe. The results showed that these substances exerted negligible interference on Ox-PGP1 compared with PGP-1, further confirming that Ox-PGP1 had high specificity to PGP-1 (Figure S12). As depicted in Figure S13, the application of iodoacetamide, an inhibitor of PGP-1, led to a significant reduction in the fluorescence intensity of the reaction system. This indicates that the enhanced fluorescence of Ox-PGP1 is caused directly by the presence of PGP-1, confirming its high specificity to PGP-1. Furthermore, in the comparative study involving iodoacetamide and three other inhibitors, iodoacetamide exhibited the most pronounced inhibition effect on PGP-1, as evidenced by fluorescence spectroscopic data.

Theoretical Calculation and Molecular Docking. The ground state geometries and electronic structures of Ox-PGP1 and oxazine 1 were scrutinized by using theoretical calculations (Figure 3A). Ox-PGP1, which lacks an extensive intramolecular conjugated structure, led to a clear separation between the HOMO and LUMO electron clouds, resulting in almost invisible absorption and emission. However, Ox-PGP1 was converted into oxazine 1 upon incubation with PGP-1, prompting the formation of large π-bonds in the molecule. This change resulted in a significant overlap between the HOMO and LUMO electron clouds in the phenoxazine structure. Time-dependent density functional theory (TDDFT) was further employed to calculate the UV−vis absorption and emission spectra. The transitions were corresponded to an absorption peak at 635.52 nm (f = 1.2962) and a fluorescence peak at 684.28 nm (f = 1.2277), in accordance with the experimental spectral results.

Molecular docking experiments were also executed to simulate the binding of Ox-PGP1 to PGP-1. As presented in Figure 3B, in the presence of PGP-1, Ox-PGP1 readily penetrated the active site of PGP-1 and combined with it. PGP-1 subsequently severed the recognition site of Ox-PGP1, leading to the release of oxazine 1 and the enhancement of the fluorescence signal. The binding energy was determined to be −8.3 kcal/mol, and Ox-PGP1 was found to form three hydrogen bonds with three amino acids (Ala106, Ser150, and Lys157) of PGP-1. These results prove that the probe Ox-PGP1 can effectively bind to PGP-1.

Thus, the transformation of Ox-PGP1 into oxazine 1, which caused the spectral changes, was confirmed through theoretical calculations and molecular docking experiments. Moreover, these findings illustrated the potent binding affinity between Ox-PGP1 and PGP-1. The sensing mechanism of Ox-PGP1 for PGP-1, as presented in Figure 3C, further strengthens these results. Overall, the results highlight the suitability and potential of Ox-PGP1 in biological imaging applications.

Cytotoxicity Assessment. Before the cell imaging of normal thyroid cells (Nthy-ori3−1 cells), the cytotoxicity of Ox-PGP1 was evaluated using a CCK8 assay. This step is crucial to ensure that the probe does not cause an inadvertent impact on the health and normal function of the cells during the imaging processes. The results demonstrated that after a 24-h incubation with various concentrations of Ox-PGP1, cell viability remained high and exceeded 90% across all tested concentrations (Figure S14). This clearly proves the low cytotoxicity of Ox-PGP1, which makes it an ideal candidate for our study. These findings also give us the necessary confidence in using the probe Ox-PGP1 in subsequent cell imaging experiments.

Endogenous and Inflammation-Induced Cell Imaging. Fluorescence was observed upon the introduction of Ox-PGP1 into Nthy-ori3−1 cells. The fluorescence intensity progressively increased with incubation time, reaching a plateau at 2 h, and thereafter remained stable (Figure S15). This appearance indicates the high stability of Ox-PGP1 in living Nthy-ori3−1 cells. Taking into account both the cell survival and fluorescence intensity, we chose a 40 min incubation time as the optimal response time for Ox-PGP1 in cells.

Subsequently, Nthy-ori3−1 cells were treated with lipopolysaccharide (LPS) at different concentrations (0.1, 0.2, and 0.5 μg/mL) for 16 h to simulate various levels of cellular inflammation. This was followed by the introduction of Ox-PGP1 for 40 min of fluorescence imaging. Distinct fluorescence emission was observed post-Ox-PGP1 addition,

https://doi.org/10.1021/acs.analchem.3c05872
Anal. Chem. 2024, 96, 5897−5905

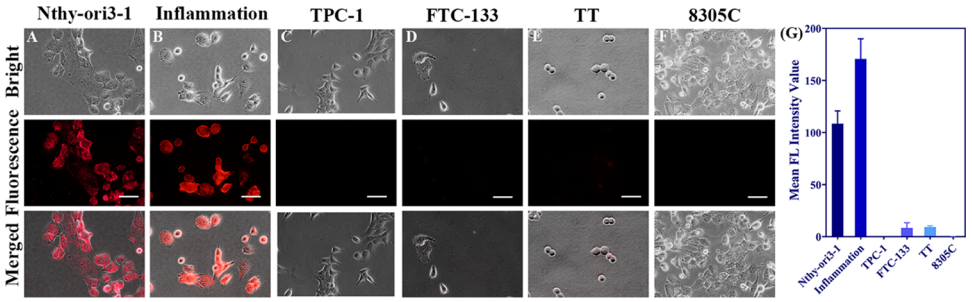

Figure 5. Fluorescence imaging of various thyroid cells under various conditions: (A) Nthy-ori3−1 cells following a 40 min incubation with 10 μM Ox-PGP1. (B) Nthy-ori3−1 cells after a 16 h incubation with 0.5 μg/mL LPS, subsequently treated with 10 μM Ox-PGP1 for 40 min. (C) TPC-1 cells after a 40 min incubation with 10 μM Ox-PGP1. (D) FTC-133 cells after a 40 min incubation with 10 μM Ox-PGP1. (E) TT cells after a 40 min incubation with 10 μM Ox-PGP1. (F) 8305C cells after a 40 min incubation with 10 μM Ox-PGP1. (G) Comparison of fluorescence intensities obtained under the above conditions. λex = 605−640 nm, λem = 670−715 nm. Scale bar, 50 μm.

signifying the normal expression level of PGP-1 in Nthy-ori3−1 cells (Figure 4). As the LPS concentration increased, the intracellular fluorescence intensity was significantly enhanced, an indication of an overexpression of PGP-1 in inflamed thyroid cells compared to that in Nthy-ori3−1 cells. These results implied that the expression of PGP-1 was upregulated as the inflammation intensified. The observations also suggest that PGP-1 could serve as an indicator for thyroiditis and could be detected by fluorescence imaging by using Ox-PGP1.

Evaluating Therapeutic Efficacy of Medications. In an attempt to identify the most effective therapeutic agent for thyroiditis, a comparative study involving four different medications was conducted. These selected medications were separately introduced to inflamed thyroid cells (induced by LPS). Each medication was allowed to interact with the cells for an hour. This was followed by the addition of Ox-PGP1 prior to fluorescence imaging. The fluorescence intensity, a crucial marker indicating the activity of PGP-1, was closely monitored and recorded. As illustrated in Figure S16, the fluorescence intensity in the cells was noticeably reduced following the administration of the four medications. This observation is in contrast to the control group, which was without any medication. Among all, the administration of iodoacetamide resulted in the most substantial decrease in fluorescence. This finding suggests that iodoacetamide has the strongest inhibitory effect on PGP-1. Furthermore, the pronounced reduction in the fluorescence intensity indirectly reveals that iodoacetamide is a potentially highly effective inhibitor of PGP-1. Additionally, this could have far-reaching implications for the treatment of thyroiditis.

Comparative Analysis of Various Thyroid Cancer Cells. We compared PGP-1 expression across several thyroid cell types, including Nthy-ori3−1 cells, inflammatory thyroid cells, and four subtypes of thyroid cancer cells: TPC-1, FTC-133, TT, and 8305C cells. These subtypes represent pathological variants of thyroid cancer, including papillary, follicular, medullary carcinomas, and undifferentiated carcinoma. Upon fluorescence imaging, a clear pattern was observed. The fluorescence intensity, which is an indicator of PGP-1 expression, in inflammatory thyroid cells was notably stronger compared to that in Nthy-ori3−1 cells. Furthermore, both the inflammatory cells and Nthy-ori3−1 cells exhibited markedly higher fluorescence than other thyroid cancer cells (Figure 5). This finding implies that Ox-PGP1 could effectively differentiate normal and inflammatory thyroid cells from various major thyroid cancer cells. This superior diagnostic capability holds great promise for Ox-PGP1 in guiding therapeutic decisions and ensuring timely treatment.

Subsequently, we simulated inflammatory conditions in thyroid cancer cells by adding LPS. TPC-1 cells, which represent the most common subtype of thyroid cancer cells, were selected. The cells were incubated with Ox-PGP1 for 40 min. As revealed in Figure S17, only a minimal fluorescence enhancement was observed in TPC-1 cells, despite the significant increase in LPS concentration. After LPS induction, the fluorescence intensity of TPC-1 cells remained substantially lower than that of Nthy-ori3−1 cells. In conclusion, the fluorescence intensity of severely inflamed TPC-1 cells was significantly lower than that of Nthy-ori3−1 cells. This finding suggests that Ox-PGP1 could be used to distinguish inflamed cancer tissues from normal tissues, and thus could be employed to prevent treatment delay due to missed diagnosis.

Imaging of Cocultured Cells. The significant difference of fluorescence intensity between normal and cancer cells led us to investigate the potential ability of Ox-PGP1 to distinguish between normal cells and cancer cells. TPC-1 cells were mixed with Nthy-ori3−1 cells and then incubated with nuclear dye Hoechst 33342 and Ox-PGP1. As depicted in Figure S18, nuclear dye (blue channel) was predominantly localized in Nthy-ori3−1 cells. By contrast, the fluorescence intensity of Ox-PGP1 (red channel) in Nthy-ori3−1 cells was significantly higher compared to that in TPC-1 cells. Taking into account both the above results and cell morphology, we concluded that cells exhibiting both blue and red fluorescence predominantly were Nthy-ori3−1 cells, while cells with weak intensity in both channels predominantly were TPC-1 cells. In Figure S18, Nthy-ori3−1 cells were highlighted and marked. These results demonstrate that the fluorescence intensity of Ox-PGP1 could be used to distinguish normal cells from cancer cells. The results also provide crucial experimental evidence for differentiating between paracancerous normal tissues and cancer tissues.

***In vivo* Imaging of Normal Mice, Autoimmune Thyroiditis, and Thyroid Carcinoma in Mice.** The remarkable spectroscopic properties of Ox-PGP1, along with its notable resolution potential for cellular imaging, position it as a promising candidate for biomedical imaging. To further explore this prospect and to effectively validate the ability of Ox-PGP1 in differentiation between different thyroid diseases *in vivo*, we established the autoimmune thyroiditis and thyroid cancer mice model. To the best of our knowledge, this was the first application of the PGP-1 probe to thyroid diseases, which

https://doi.org/10.1021/acs.analchem.3c05872
Anal. Chem. 2024, 96, 5897−5905

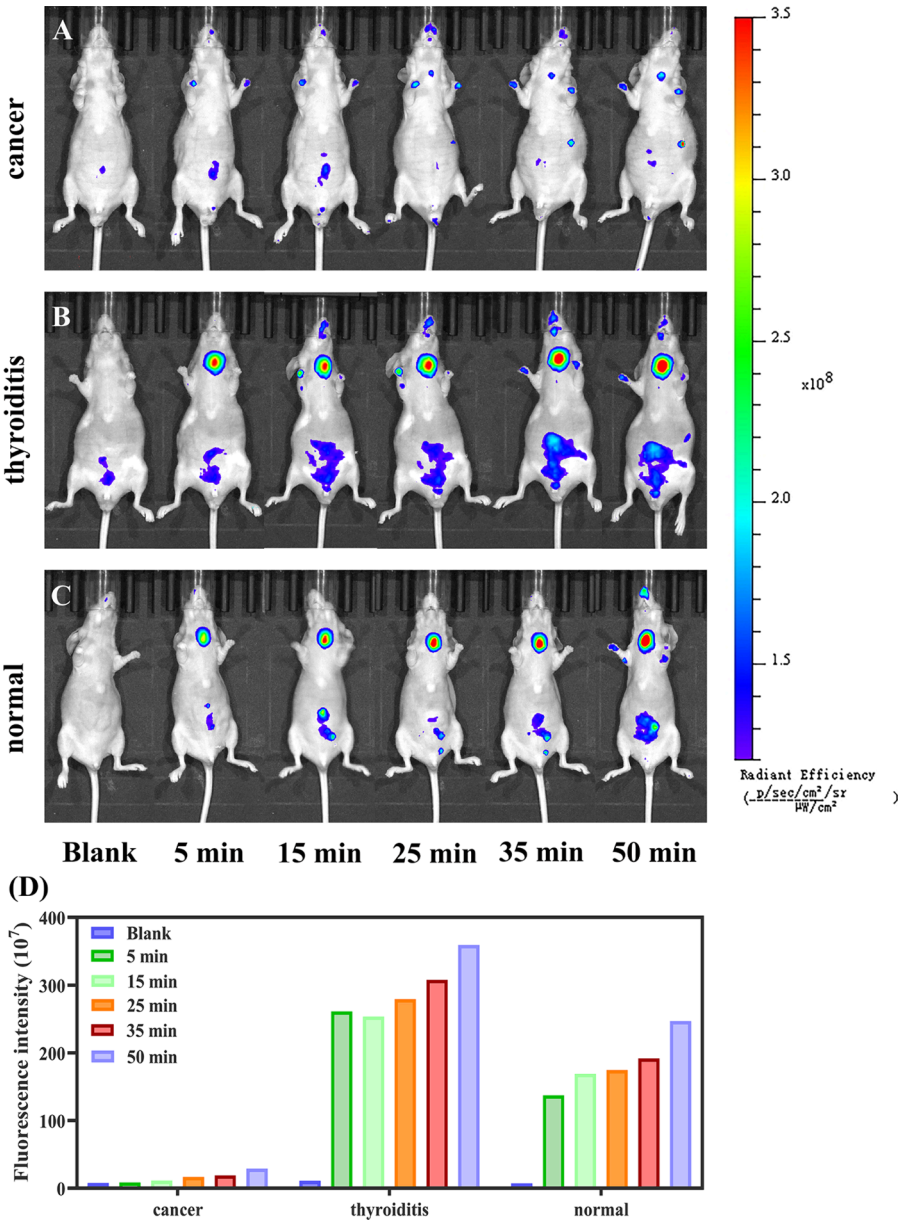

Figure 6. Fluorescence images of thyroid cancer, autoimmune thyroiditis, and normal mice injected with Ox-PGP1 (60 μM, 200 μL) after varying time: (A) thyroid cancer mouse, (B) autoimmune thyroiditis mouse, and (C) normal mouse. (D) Comparison of fluorescence intensities of mice under different diseases states.

would be a completely novel exploration (Table S1). Ox-PGP1 was injected near the neck of the mice (without the need for advanced tissue-targeting technology) with a specific aim to swiftly and effectively target the thyroid gland and to facilitate the fluorescence imaging. This easy and convenient strategic placement ensures the specific localization of Ox-PGP1 and its enhanced interaction with the targeted thyroid tissues. It was a wonder that as depicted in Figure 6, mice in the autoimmune thyroiditis group exhibited a markedly strong fluorescence signal at the thyroid site a mere 5 min following Ox-PGP1 injection (Figure 6B2), as compared to that without Ox-PGP1 injection (Figure 6B1). In contrast, the thyroid cancer mice presented only a faint fluorescence signal (Figure 6A2). The fluorescence intensity at the thyroid site of normal mice was moderate, between the intensity of cancerous and thyroiditis mice (Figure 6C2). This is consistent with the results from the above cellular experiments.

After an extended period of time, a slight increase in the fluorescence signal was observed in mice in the same group (Figure 6D). However, comparing the fluorescence signals of normal, thyroiditis, and cancerous mice after an extended period of time, the intercontrast relationship of the fluorescence signals of mice in the above three was found to remain consistent with that of the fluorescence signals at 5 min. This indicates that although the fluorescence signals of these three mice were slightly stronger as time was extended, the exposure time of 5 min was sufficient to demonstrate the suitability of Ox-PGP1 for detecting and differentiating between different thyroid states. This was the most extremely fast tool in comparison to the previous literature in Table S1, and it was first applied for the detection and differentiation based on the fluorescence intensity at the thyroid site *in vivo*, which implied great potential.

https://doi.org/10.1021/acs.analchem.3c05872
Anal. Chem. 2024, 96, 5897−5905

The strong difference in fluorescence signals observed within a short period of time suggests that Ox-PGP1 could rapidly and effectively detect and differentiate between thyroid diseases *in vivo*. It also implies that Ox-PGP1 could potentially serve as a highly sensitive and rapid diagnostic tool for the noninvasive diagnosis of targeted organs.

CONCLUSIONS

In conclusion, we successfully engineered a novel NIR probe, Ox-PGP1, with superior specificity for PGP-1 detection. Due to the oxazine 1 fluorophore, Ox-PGP1 had outstanding photostability and enhanced fluorescence by nearly 18-fold upon interacting with PGP-1. The high specificity of Ox-PGP1 to PGP-1 allowed for the precise identification of PGP-1, and interference from other prevalent biomolecules in biological systems had almost no effect on the identification. At the cellular level, Ox-PGP1 was proven to be a powerful tool for the screening and effective treatment of thyroiditis. Moreover, Ox-PGP1 showed potential in differentiating normal thyroid cells from cancerous cells. Finally, Ox-PGP1 demonstrated the capacity in sensitive and rapid differentiation between autoimmune thyroiditis and thyroid carcinoma by extending its application beyond *in vivo* detection. Taken together, the ability of this novel Ox-PGP1 to accurately and rapidly detect Ox-PGP1 provides it with a substantial advantage over traditional imaging and other detection methods. The tool can potentially be utilized to improve earlier interventions and thyroid patient outcomes.

ASSOCIATED CONTENT

Supporting Information

The Supporting Information is available free of charge at https://pubs.acs.org/doi/10.1021/acs.analchem.3c05872.

Materials and instruments, enzymatic kinetics assays, theoretical calculation, molecular docking, CCK8 assay, cell culture procedures, cell imaging procedures and supplementary figures, table, and references (PDF)

AUTHOR INFORMATION

Corresponding Authors

Pinyi Ma − *College of Chemistry, Jilin Province Research Center for Engineering and Technology of Spectral Analytical Instruments, Jilin University, Changchun 130012, China;* orcid.org/0000-0002-3230-4928; Email: mapinyi@jlu.edu.cn

Hui Han − *Thyroid Surgery Department, General Surgery Center, First Hospital of Jilin University, Changchun 130012, China*; Email: hanhuijdyy@jlu.edu.cn

Daqian Song − *College of Chemistry, Jilin Province Research Center for Engineering and Technology of Spectral Analytical Instruments, Jilin University, Changchun 130012, China;* orcid.org/0000-0002-4866-1292; Email: songdq@jlu.edu.cn

Authors

Siqi Zhang − *College of Chemistry, Jilin Province Research Center for Engineering and Technology of Spectral Analytical Instruments, Jilin University, Changchun 130012, China*

Mo Ma − *College of Chemistry, Jilin Province Research Center for Engineering and Technology of Spectral Analytical Instruments and School of Pharmacy, Jilin University, Changchun 130012, China*

Jingkang Li − *College of Chemistry, Jilin Province Research Center for Engineering and Technology of Spectral Analytical Instruments, Jilin University, Changchun 130012, China*

Jiaxin Li − *College of Chemistry, Jilin Province Research Center for Engineering and Technology of Spectral Analytical Instruments, Jilin University, Changchun 130012, China*

Lanlan Xu − *College of Chemistry, Jilin Province Research Center for Engineering and Technology of Spectral Analytical Instruments, Jilin University, Changchun 130012, China*

Dejiang Gao − *College of Chemistry, Jilin Province Research Center for Engineering and Technology of Spectral Analytical Instruments, Jilin University, Changchun 130012, China*

Complete contact information is available at: https://pubs.acs.org/10.1021/acs.analchem.3c05872

Notes

The authors declare no competing financial interest.

ACKNOWLEDGMENTS

This work was supported by the National Natural Science Foundation of China (22004046 and 22074052) and the Science and Technology Developing Foundation of Jilin Province of China (nos. 20230101033JC, 20220505015ZP, and YDZJ202302CXJD031).

REFERENCES

(1) Ferrari, S. M.; Ragusa, F.; Elia, G.; Paparo, S. R.; Mazzi, V.; Baldini, E.; Benvenga, S.; Antonelli, A.; Fallahi, P. *Front. Pharmacol.* **2021**, *12*, No. 750380.

(2) de Luis, D.; Varela, C.; Sancho Rof, J. M. *Rev. Clin. Esp.* **1997**, *197*, 640−642.

(3) Zhao, L.; Liu, Y.; Su, H.; Shi, X. *Medicine* **2021**, *100*, No. e26273.

(4) Santoro, D.; Vadalà, C.; Siligato, R.; Buemi, M.; Benvenga, S. *Front. Endocrinol.* **2017**, *8*, 119.

(5) Bortun, A. C.; Ivan, V.; Navolan, D. B.; Dehelean, L.; Borlea, A.; Stoian, D. *J. Clin. Med.* **2021**, *10*, 369.

(6) Daramjav, N.; Takagi, J.; Iwayama, H.; Uchino, K.; Inukai, D.; Otake, K.; Ogawa, T.; Takami, A. *Medicina* **2023**, *59*, 757.

(7) Noureldine, S. I.; Tufano, R. P. *Curr. Opin. Oncol.* **2015**, *27*, 21−25.

(8) Debbaut, A.; Gilliaux, O. *Arch. Pediatr.* **2023**, *30*, 131−135.

(9) Farrell, E.; Heffron, C.; Murphy, M.; O'Leary, G.; Sheahan, P. *Head Neck-J. Sci. Spec.* **2017**, *39*, 122−127.

(10) Kakudo, K.; Bai, Y.; Katayama, S.; Hirokawa, M.; Ito, Y.; Miyauchi, A.; Kuma, K. *Pathol. Int.* **2009**, *59*, 359−367.

(11) Ralli, M.; Angeletti, D.; Fiore, M.; D'Aguanno, V.; Lambiase, A.; Artico, M.; de Vincentiis, M.; Greco, A. *Autoimmunity Rev.* **2020**, *19*, No. 102649.

(12) Gordin, A.; Lamberg, B. A. *Clin. Endocrinol.* **1981**, *15*, 537−543.

(13) LiVolsi, V. A. *Thyroid: official journal of the American Thyroid Association* **1994**, *4*, 333−339.

(14) Zefirova, G. S.; Ibragimova, G. V.; Kondrat'eva, L. V.; Shchepetkova, L. V.; Davitinidze, N. L. *Terapevt. Arkh.* **1984**, *56*, 66−70.

(15) Fink, H.; Hintze, G. *Med. Klin.* **2010**, *105*, 485−493.

(16) Wu, Z. G.; Yan, X. Q.; Su, R. S.; Ma, Z. S.; Xie, B. J.; Cao, F. L. *World J. Surg.* **2017**, *41*, 129−135.

(17) Stasiak, M.; Michalak, R.; Lewinski, A. *BMC Endocr. Disord.* **2019**, *19*, 86.

(18) Kumarasinghe, M. P.; De Silva, S. *Pathology* **1999**, *31*, 1−7.

(19) Wang, D.; Tang, B. Z. *Acc. Chem. Res.* **2019**, *52*, 2559−2570.

(20) Zhang, J.; Chai, X.; He, X.-P.; Kim, H.-J.; Yoon, J.; Tian, H. *Chem. Soc. Rev.* **2019**, *48*, 683−722.

(21) Jin, X.; Wu, X.; Xie, P.; Liu, S.; Wu, J.; Wang, T.; Zhou, H.; Leng, X.; Chen, W. *Anal. Methods* **2018**, *10*, 4079−4084.

(22) Xu, L.; Chu, H.; Gao, D.; Wu, Q.; Sun, Y.; Wang, Z.; Ma, P.; Song, D. *Anal. Chem.* **2023**, *95*, 2949−2957.
(23) Li, J.; Cao, J.; Wu, W.; Xu, L.; Zhang, S.; Ma, P.; Wu, Q.; Song, D. *Sensor. Actuat. B-Chem.* **2023**, *377*, No. 133122.
(24) Qian, J.; Teng, Z.; Wang, J.; Zhang, L.; Cao, T.; Zheng, L.; Cao, Y.; Qin, W.; Liu, Y.; Guo, H. *Acs. Sens.* **2020**, *5*, 2806−2813.
(25) Gong, Q.; Li, L.; Wu, X.; Ma, H. *Chem. Sci.* **2016**, *7*, 4694−4697.
(26) Guo, W.-Y.; Li, R.-R.; Fu, Y.-X.; Liu, S.-Y.; Liu, G.-Z.; Yang, W.-C.; Yang, G.-F. *Anal. Chem.* **2021**, *93*, 13311−13318.
(27) Gong, Q.; Zou, R.; Xing, J.; Xiang, L.; Zhang, R.; Wu, A. *Adv. Sci.* **2018**, *5*, 1700664.
(28) Chelius, D.; Jing, K.; Lueras, A.; Rehder, D. S.; Dillon, T. M.; Vizel, A.; Rajan, R. S.; Li, T. S.; Treuheit, M. J.; Bondarenko, P. V. *Anal. Chem.* **2006**, *78*, 2370−2376.
(29) Chatterton, D. E. W.; Nguyen, D. N.; Bering, S. B.; Sangild, P. T. *Int. J. of Biochem. Cell Biol.* **2013**, *45*, 1730−1747.
(30) Suzuki, Y.; Motoi, H.; Sato, K. *J. Agric. Food Chem.* **1999**, *47*, 5297−5297.
(31) Awade, A. C.; Cleuziat, P.; Gonzales, T.; Robert-Baudouy, J. *Proteins* **1994**, *20*, 34−51.
(32) Abe, K.; Fukuda, K.; Tokui, T. *Biol. Pharm. Bull.* **2004**, *27*, 1197−1201.
(33) Zhang, P.; Fu, C.; Liu, H.; Guo, X.; Zhang, Q.; Gao, J.; Chen, W.; Yuan, W.; Ding, C. *Anal. Chem.* **2021**, *93*, 11337−11345.
(34) Shang, J.; Zhang, X.; He, Z.; Shen, S.; Liu, D.; Shi, W.; Ma, H. *Angew. Chem., Int. Ed.* **2022**, *61*, e202205043.
(35) Zaccone, P.; Fehervari, Z.; Blanchard, L.; Nicoletti, F.; Edwards, C. K.; Cooke, A. *Eur. J. Immunol.* **2002**, *32*, 1021−1028.

https://doi.org/10.1021/acs.analchem.3c05872
Anal. Chem. 2024, 96, 5897−5905